Supporting Information

QM/MD studies on graphene growth from small islands on Ni(111) surface

Menggai Jiao,[a,c] Wei Song,[b] Hu-Jun Qian,[d] Ying Wang,*[a] Zhijian Wu,*[a] Stephan Irle[e] and Keiji Morokuma[f]

[a]State Key Laboratory of Rare Earth Resource Utilization, Changchun Institute of Applied Chemistry, Chinese Academy of Sciences, Changchun 130022, China

[b]Physics and Electronic Engineering Department, Xinxiang University, Xinxiang, 453003, China

[c]University of Chinese Academy of Sciences, Beijing 100049, China

[d]State Key Laboratory of Theoretical and Computational Chemistry, Institute of Theoretical Chemistry, Jilin University, Changchun 130023, China

[e]Institute of Transformative Bio-Molecules (WPI-ITbM) and Department of Chemistry, Graduate School of Science, Nagoya University, Nagoya 464-8602, Japan

[f]Fukui Institute for Fundamental Chemistry, Kyoto University, Kyoto 606-8103, Japan

*E-mail: ywang_2012@ciac.ac.cn; zjwu@ciac.ac.cn

Contents

1. **Extended Discussion**
2. **References**

Movies:

There are two movies showing simulation process and they are provided in separate files.

Movie S1. Evolution of QM/MD simulations of the growth of graphene from one C_{13} on Ni(111) surface for trajectory D@C_{13}. Brown and cyan spheres represent Ni and C atoms, respectively. The preexisting C_{13} is highlighted in blue.

Movie S2. Evolution of QM/MD simulations of the growth of graphene from two C_{13} species on Ni(111) surface for trajectory C@2C_{13}. Color conventions as in Movie S1. The preexisting two C_{13} species are highlighted in blue and purple, respectively.

Figures:

Fig. S1 Optimized geometries of C_{13}-G and C_{13}-H on Ni(111) surface.

Fig. S2 Final structures of trajectories A-J@C_{13} following 400 ps QM/MD simulation for the Ni(111)+C_{13} system. Brown and cyan spheres represent Ni and C atoms, respectively. The preexisting C_{13} is highlighted in blue.

Fig. S3 Final structures of trajectories A-J@2C_{13} following 350 ps QM/MD simulation for the Ni(111)+2C_{13} system. Color conventions as in Fig. S1. The preexisting two C_{13} species are highlighted in blue and purple, respectively.

Fig. S4 Average polygonal carbon ring populations formed during graphene growth from (a) Ni(111)+C_{13} and (b) Ni(111)+2C_{13} systems.

Fig. S5 Averaged δ value of (a) the C_{13} clusters and (b) the nickel catalyst in Ni(111)+C_{13} and Ni(111)+2C_{13} systems, respectively.

Fig. S6 Total Mermin free energy as a function of simulation time in Ni(111)+2C_{13} system.

Tables:

Table S1. Formation energy of C_{13}-G and C_{13}-H on Ni(111) surface.

Table S2. The effect of T_e on the crystalline features of the Ni(111) surface.

1. Extended Discussion

To investigate the high mobility of C_{13} and the nickel catalyst, the Lindemann index, δ,[1] was calculated according to the following equation,

$$\delta = \frac{1}{N(N-1)} \sum_{i<j} \frac{\sqrt{\left\langle r_{ij}^2 \right\rangle_T - \left\langle r_{ij} \right\rangle_T^2}}{\left\langle r_{ij} \right\rangle_T}$$

where N is the number of atoms in the relevant system, r_{ij} is the instantaneous distance between atoms i and j, and the brackets denote thermal averaging over a finite interval of time. The Lindemann index has been used on a number of occasions as an accurate probe of the catalyst phase in the context of the nucleation and growth of graphene and carbon nanotube.[2-5] It is typically accepted that δ = 0.1 marks the transition between the solid and liquid phases.[6] Fig. S5 shows that in the two systems both the carbon clusters and the nickel catalyst rapidly undergo a solid to liquid phase transition upon thermal annealing, as indicated by the rapid increase of δ. Thus, they exhibit significantly high mobility, which is responsible for the quick diffusion and further aggregation of carbon clusters.

2. References

1. F. A. Lindemann, *Phys. Z.*, 1910, **11**, 609-612.
2. F. Ding, A. Rosén, S. Curtarolo and K. Bolton, *Appl. Phys. Lett.*, 2006, **88**, 133110.
3. A. J. Page, H. Yamane, Y. Ohta, S. Irle and K. Morokuma, *J. Am. Chem. Soc.*, 2010, **132**, 15699-15707.
4. M. Jiao, K. Li, W. Guan, Y. Wang, Z. Wu, A. Page and K. Morokuma, *Sci. Rep.*, 2015, **5**, 12091.
5. H.-B. Li, A. J. Page, C. Hettich, B. Aradi, C. Kohler, T. Frauenheim, S. Irle and K. Morokuma, *Chem. Sci.*, 2014, **5**, 3493-3500.
6. Y. Zhou, M. Karplus, K. D. Ball and R. S. Berry, *J. Chem. Phys.*, 2002, **116**, 2323-2329.

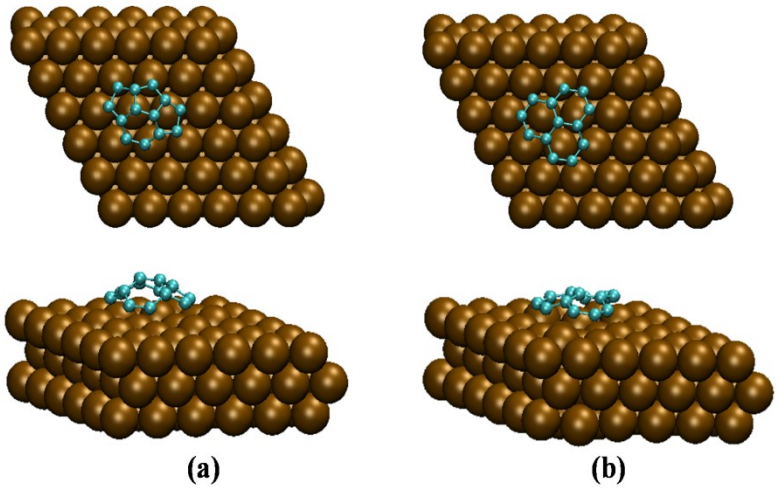

Fig. S1 Optimized geometries of C_{13}-G and C_{13}-H on Ni(111) surface.

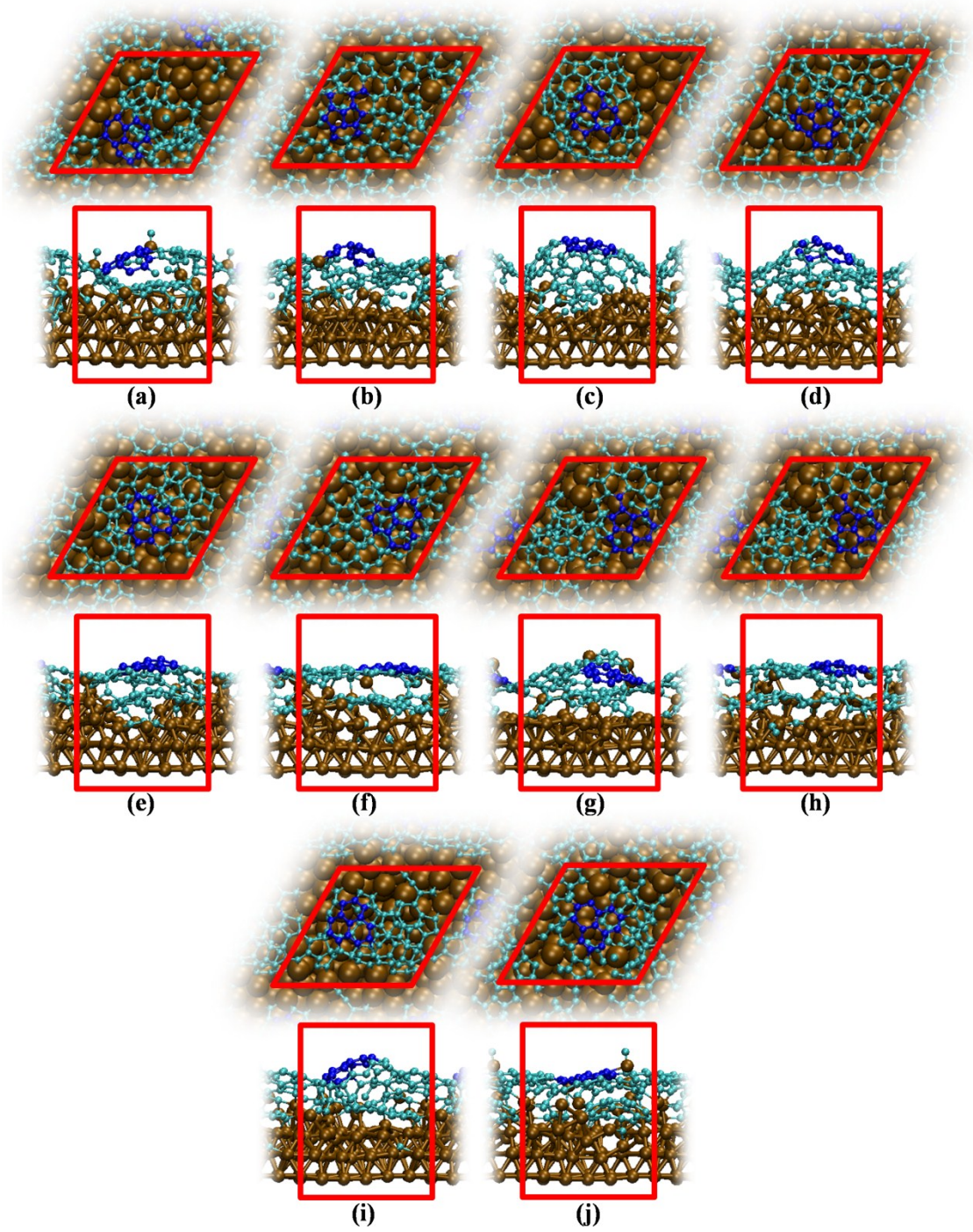

Fig. S2 Final structures of trajectories A-J@C_{13} following 400 ps QM/MD simulation for the Ni(111)+C_{13} system. Brown and cyan spheres represent Ni and C atoms, respectively. The preexisting C_{13} is highlighted in blue.

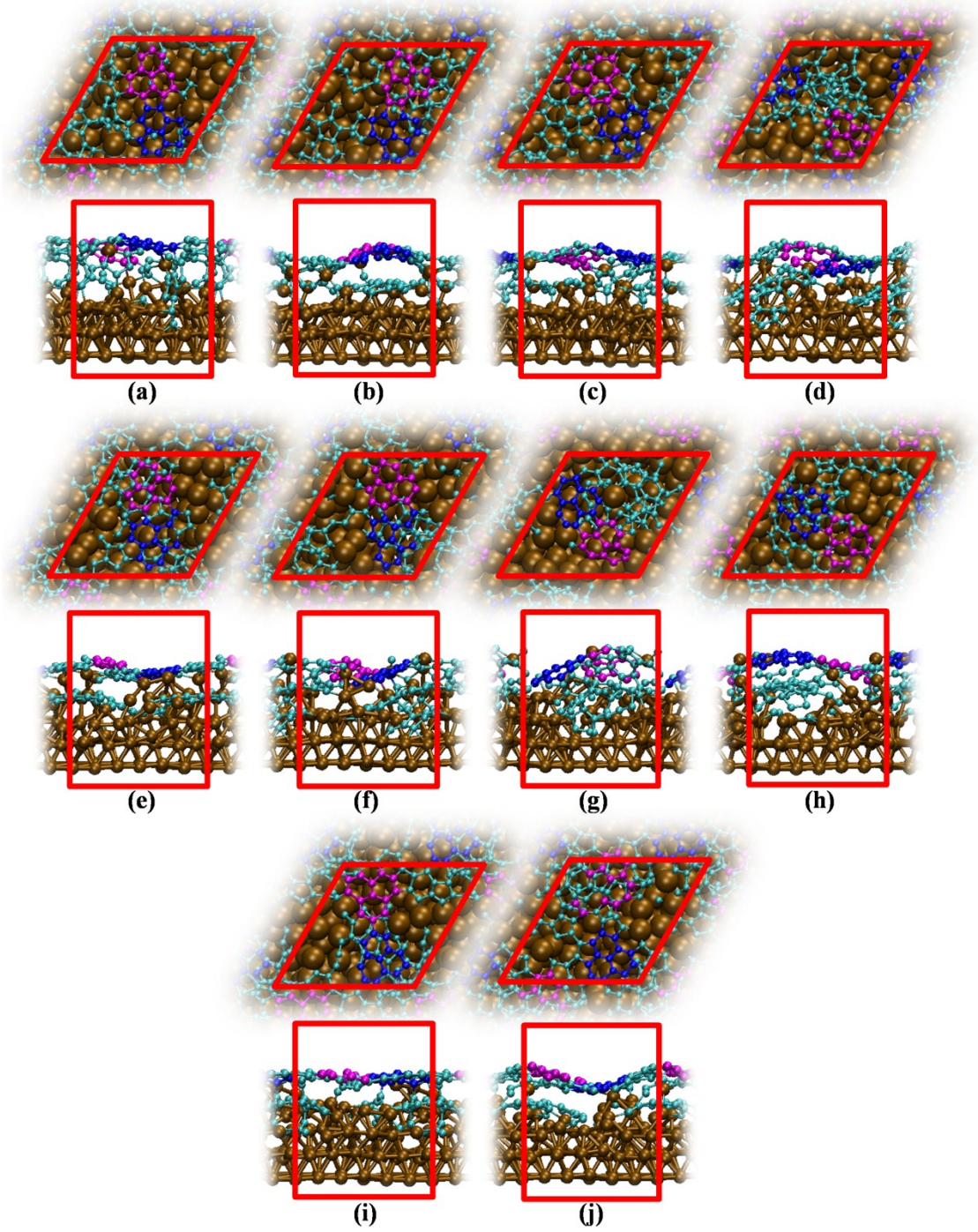

Fig. S3 Final structures of trajectories A-J@2C_{13} following 350 ps QM/MD simulation for the Ni(111)+2C_{13} system. Color conventions as in Fig. S1. The preexisting two C_{13} species are highlighted in blue and purple, respectively.

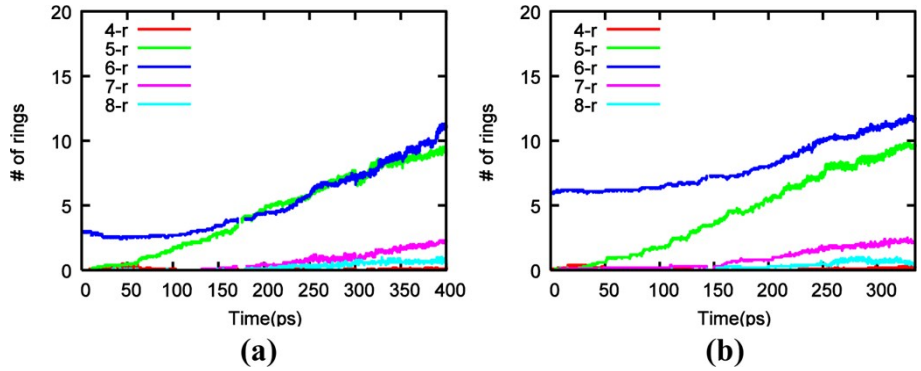

Fig. S4 Average polygonal carbon ring populations formed during graphene growth from (a) Ni(111)+C_{13} and (b) Ni(111)+2C_{13} systems.

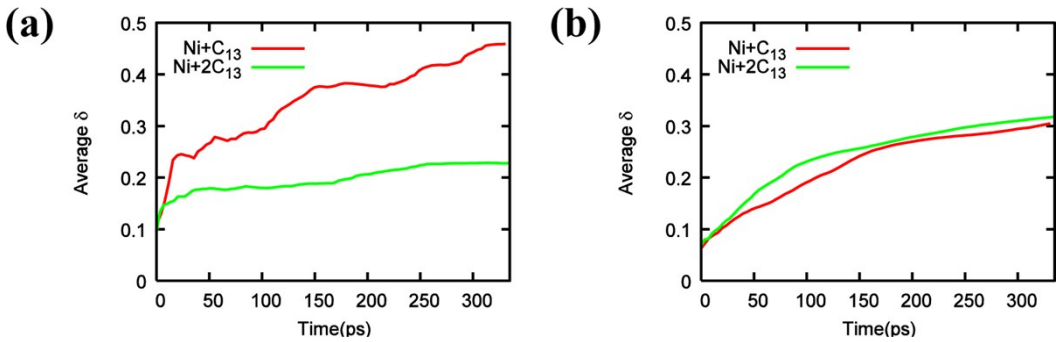

Fig. S5 Averaged δ value of (a) the C_{13} clusters and (b) the nickel catalyst in Ni(111)+C_{13} and Ni(111)+2C_{13} systems, respectively.

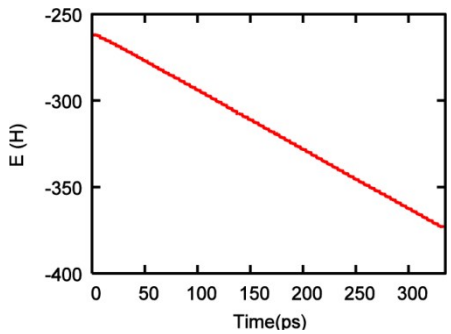

Fig. S6 Total Mermin free energy as a function of simulation time in Ni(111)+2C_{13} system.

Table S1. Formation energy of C_{13}-G and C_{13}-H on Ni(111) surface.

	C_{13}-G	C_{13}-H
DFT[a]	10.55	12.52
SCC-DFTB	14.11	15.85

[a] Ref. 22

Table S2. The effect of T_e on the crystalline features of the Ni(111) surface.

T_e (K)	a (Å)	b (Å)	c (Å)	Interlayer distance (Å)	Ni-Ni bond length (Å)
initial	14.951	14.951	6.104	2.035	2.492
500	14.934	14.934	6.442	2.147	2.489
1000	14.934	14.934	6.454	2.151	2.489
1180	14.934	14.934	6.457	2.152	2.489
1500	14.934	14.934	6.464	2.155	2.489
2000	14.934	14.934	6.480	2.160	2.489
3000	14.934	14.934	6.520	2.173	2.489
5000	14.934	14.934	6.606	2.202	2.489
6000	14.854	14.894	8.032	2.677	2.478/2.482
7000	14.926	14.855	7.081	2.360	2.488/2.476
10000	14.995	14.827	9.295	3.098	2.499/2.471